ACSNANO

www.acsnano.org

ARTICLE

Multimodal Artificial Neurological Sensory–Memory System Based on Flexible Carbon Nanotube Synaptic Transistor

Haochuan Wan, Junyi Zhao, Li-Wei Lo, Yunqi Cao, Nelson Sepúlveda, and Chuan Wang*

Cite This: *ACS Nano* 2021, 15, 14587–14597

Read Online

ACCESS | Metrics & More | Article Recommendations | Supporting Information

ABSTRACT: As the initial stage in the formation of human intelligence, the sensory–memory system plays a critical role for human being to perceive, interact, and evolve with the environment. Electronic implementation of such biological sensory–memory system empowers the development of environment-interactive artificial intelligence (AI) that can learn and evolve with diversified external information, which could potentially broaden the application of the AI technology in the field of human–computer interaction. Here, we report a multimodal artificial sensory–memory system consisting of sensors for generating biomimetic visual, auditory, tactile inputs, and flexible carbon nanotube synaptic transistor that possesses synapse-like signal processing and memorizing behaviors. The transduction of physical signals into information-containing, presynaptic action potentials and the synaptic plasticity of the transistor in response to single and long-term action potential excitations have been systematically characterized. The bioreceptor-like sensing and synapse-like memorizing behaviors have also been demonstrated. On the basis of the memory and learning characteristics of the sensory–memory system, the well-known psychological model describing human memory, the "multistore memory" model, and the classical conditioning experiment that demonstrates the associative learning of brain, "Pavlov's dog's experiment", have both been implemented electronically using actual physical input signals as the sources of the stimuli. The biomimetic intelligence demonstrated in this neurological sensory–memory system shows its potential in promoting the advancement in multimodal, user-environment interactive AI.

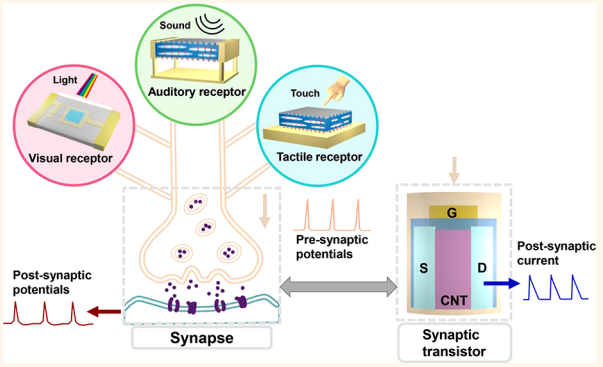

KEYWORDS: *multimodal sensing, synaptic transistor, biomimetic memory/learning, environment-interactive, artificial intelligence*

Downloaded via STANFORD UNIV on May 17, 2026 at 01:22:18 (UTC).
See https://pubs.acs.org/sharingguidelines for options on how to legitimately share published articles.

For many years, artificial intelligence has been striving to imitate and reproduce the abilities of the human brain to perform critical and sophisticated tasks such as decision-making, reasoning, and learning. These logic and cognitive functions of brain, however, are not innate and stationary. Just as other living animals, the neural system of human being will persistently evolve over the progression of its surrounding ecological and social environment through physical (visual, auditory, somatosensory, *etc.*) contacts and interactions, which are majorly enabled by the human sensory system. Such evolution of human intelligence is considered fundamentally as a memory-based process.[1] The sensory information from different sensory receptors will be integrated, processed, and memorized in the neural system, which could serve as the key factor in implementing consequential decision, cognition, or learning/memory tasks.

Due to the special structural and functional characteristics of sensory receptors, neurons, and synapses, it is hard to faithfully emulate the biological sensory and memory nervous systems in traditional von Neumann architecture without costing considerable computational resources.[2] Thus, new approaches to artificial intelligence have sprung from the idea that intelligence can emerge as much from artificial sensory–memory system consisting of biomimetic sensors and synaptic devices as it does from artificial neural network algorithms and models. Because of the advancement in microelectronic design and fabrication technologies, the artificial sensory–memory systems can even be achieved in flexible formats.[3]

Received: May 20, 2021
Published: September 2, 2021

© 2021 American Chemical Society

https://doi.org/10.1021/acsnano.1c04298
ACS Nano 2021, 15, 14587–14597

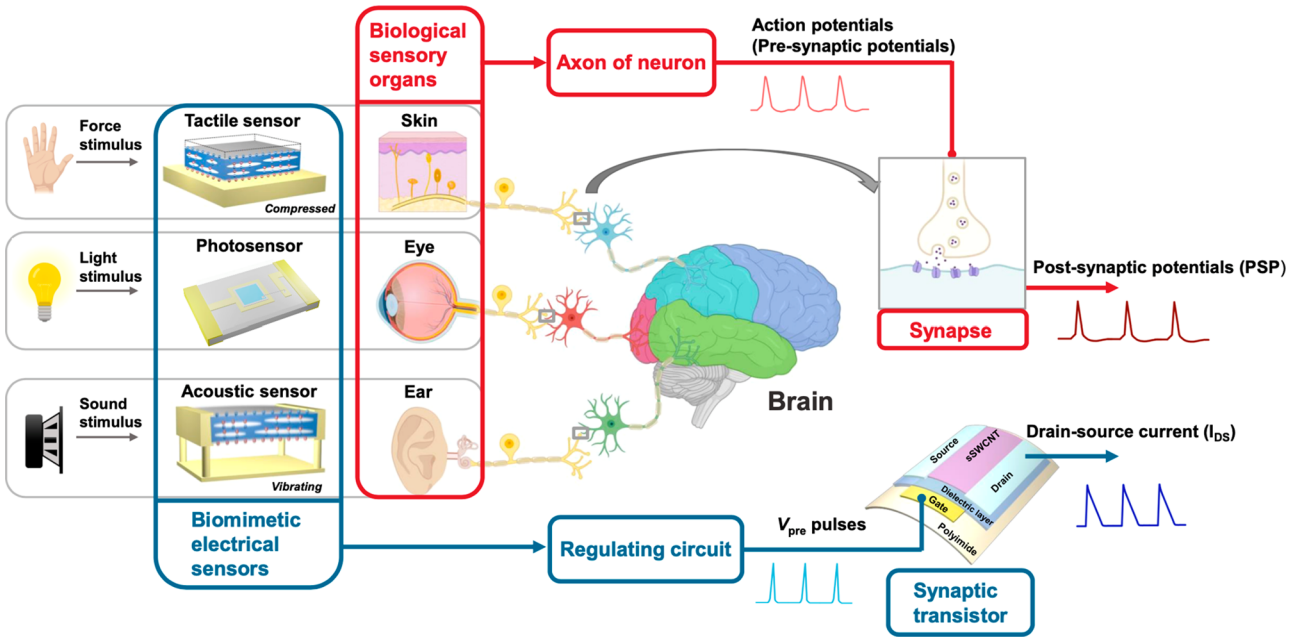

Figure 1. Schematic illustration of biological visual, auditory, and tactile sensory organs and process of information transmission and storage through neuron and synapse (circled and highlighted in red), in comparison with the artificial sensory−memory system consisting of corresponding biomimetic physical sensors and artificial synaptic transistor (circled and highlighted in blue). The schematic illustration is partially created with BioRender.com.

In the human sensory system, four types of sensory receptors constitute the foundation of five basic human senses (sight, hearing, touch, smell, and taste): photoreceptors, mechanoreceptors, thermoreceptors, and chemoreceptors.[4] Among the different categories of receptors, photoreceptors are specialized in visual phototransduction and are concentrated around center of the retina, whereas the mechanoreceptors are more widely distributed around the human body. The mechanoreceptors can be found in the human skin to transduce touch and stretch and in the ear to transduce sound. The electronic analogues of photoreceptors can be readily implemented by photodetectors[5,6] or photosensitized synaptic devices.[7,8] The realization of electronic mechanoreceptors, on the other hand, prefers a versatile device that can transduce mechanical signal in different forms. Among the flexible artificial mechanoreceptors based on change of resistance,[9] change of capacitance,[10] piezoelectricity,[11] or triboelectricity,[12] polypropylene-based ferroelectret nanogenerator (FENG) has been demonstrated to be efficient in generating pulsed electrical signals in response to tactile stimuli,[13] which closely mimics the biological sensing mechanism. Moreover, due to the large electromechanical transformation efficiency (d_{33} of ~300 pC/N)[14] and low Young's modulus (~1×10^6 N·m^{-2}),[15] FENG has also shown the capability as a multifunctional mechanoreceptor that responds not only to touch[16] but also to sound vibration.[17]

When the sensory receptors receive external stimuli, they will first transduce different forms of physical stimuli into information-encoded, brain-interpretable electrical pulses called "action potentials", as shown in Figure 1. The action potentials will then be passed along the axon of the neuron to central neural system to be processed. The synapse, functioning as an essential structure between the input (presynaptic) neuron and the target (postsynaptic) neuron, permits the transmission of action potentials from one neuron to another. The synapse also possesses the ability to adjust its own strength (synaptic weight) in response to the information contained in the input action potentials and will maintain that change of strength even after the extinction of input. Such a behavior is generally known as "synaptic plasticity", and it is widely accepted as one of the fundamental cellular mechanisms that underlie the formation of memory and learning operations in human brain.[18] The structure and behavior of the biological synapse can be emulated by synaptic transistor in which the synaptic weight is represented by the channel conductance. The modification of channel conductance in response to the pulsed gate signals can be regarded as the electronic analogue of synaptic plasticity, which leads to the artificial synapse-like memory.

In this study, an artificial multimodal sensory−memory system has been developed and endowed with bioreceptor-like sensory capability and synaptic-like memory to mimic the biological sensory−memory behaviors. Three out of the five human basic sensing abilities (touch, hearing, and sight) are enabled by utilizing FENG as both tactile sensor and acoustic sensor and phototransistor as optical sensor. The physical stimuli are converted to information-containing electrical pulses and then relayed through regulating circuits into the artificial nervous system, represented by the flexible semiconducting single-wall carbon nanotube (sSWCNT) synaptic thin-film transistor, to be processed and stored. The synaptic weight response behaviors (synaptic plasticity) of the artificial synaptic transistor to single-pulse stimulus and continuous, long-term stimuli from visual, auditory, and tactile-induced electrical pulses with different input stimulus intensities have been systematically studied to characterize the dynamic modification profiles of the synaptic memory. On the basis of this sensory−memory system, we manage to reproduce some well-known human memory and learning models. The multistore model of memory (Atkinson−Shiffrin memory model), which describes the memory states transition from short-term memory to long-term memory through rehearsal, is

https://doi.org/10.1021/acsnano.1c04298
ACS Nano 2021, 15, 14587−14597

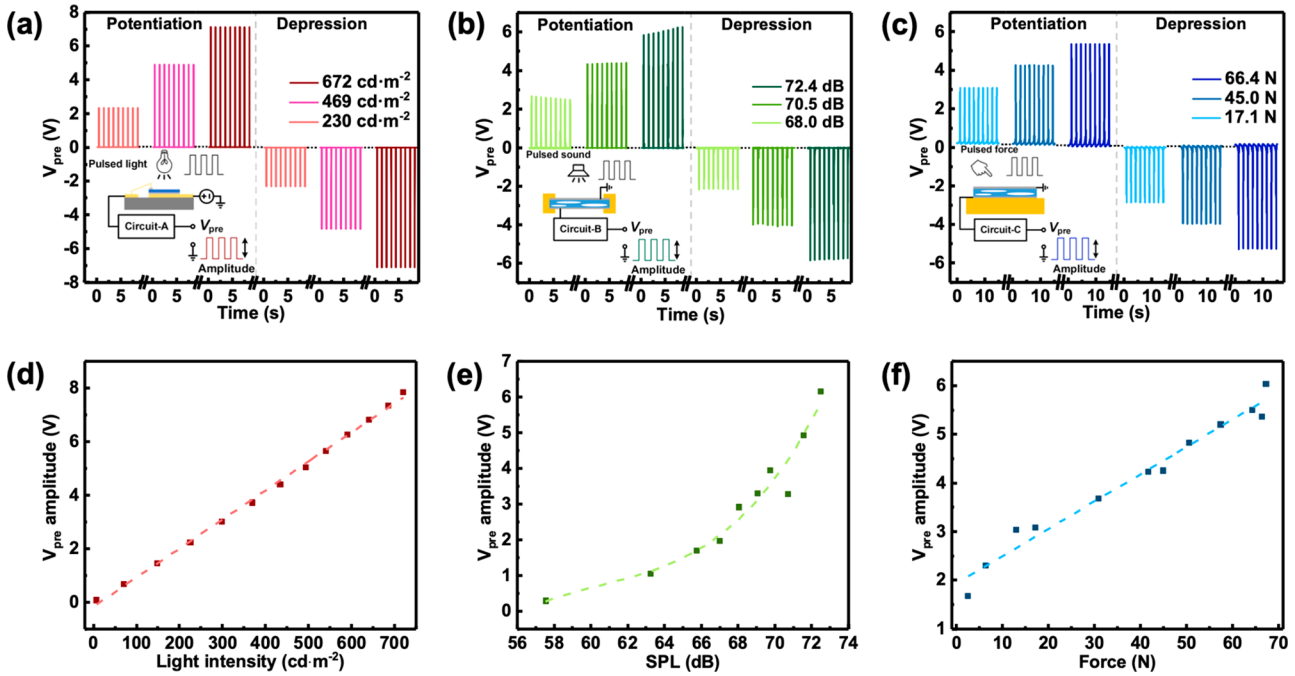

Figure 2. Transduction characterizations of the multimodal sensory system. Potentiation (positive) and depression (negative) presynaptic pulses (V_{pre}) induced by (a) visual stimuli, (b) auditory stimuli, and (c) tactile stimuli. Inset of each figure shows a simplified illustration of the corresponding transduction process. (d) Plot of the amplitudes of visual V_{pre} versus the light intensities of input visual stimuli. (e) Plot of the amplitudes of auditory V_{pre} versus the SPLs of input auditory stimuli. (f) Plot of the amplitudes of tactile V_{pre} versus the forces of input tactile stimuli. In panels d–f, the dashed lines represent the fitting curve with the fitting equations shown in Table S1.

imitated by applying sequences of visual stimuli with different number of repetitions and different light intensities. The classical conditioning experiment (Pavlov's dog experiment), which established the associative learning model, is also investigated by synergizing visual and auditory stimuli and monitoring the learning behavior of the synaptic transistor in response to the individual and interrelated stimuli. The "brain-like" intelligence achieved through this artificial multimodal sensory–memory system may be used for imitating multiplex and multifunctional biological sensory and nervous system and may facilitate the construction of environment-interactive artificial intelligence.

RESULTS AND DISCUSSION

The pulsed electrical output signals from the visual, auditory, and tactile sensory circuit are presented in panels a, b, and c of Figure 2a, respectively. In a sensory–memory system, the sensory transduction process can be regarded as the "presynaptic" process. The electrical pulses generated from these sensory circuits will eventually be relayed to the artificial synapse to be processed; thus these electrical pulses (action potentials) can also be called presynaptic pulses (V_{pre}). As shown in Figure 1, these sensory circuits are analogous to the photoreceptors and mechanoreceptors in biological sensory organs such as eye, ear, and skin. According to the types of input signal, the output V_{pre} can be categorized into visual V_{pre}, auditory V_{pre}, and tactile V_{pre}.

As illustrated in the inset of Figure 2a, a periodical sequence of light pulses representing the visual stimuli can be transduced into the corresponding sequence of visual V_{pre} through an ambient-light phototransistor and the regulating circuit-A (circuit diagram in Figure S1a). The detailed diagrams of phototransistor are shown in Figure S1b,c, and the details of the generation of visual stimuli and the visual V_{pre} are summarized in Table S1. For biomimetic synaptic weight modulation, both potentiation pulses (pulses that cause the increase of the synaptic weight) and depression pulses (pulses that cause decrease of the synaptic weight) are required, and the potentiation–depression pulses pair are usually represented by electrical pulses with opposite polarities. This can be realized by interchanging the output terminals of the regulating circuit-A through a switch, whereas for integrated optoelectronic synaptic device, a combination of light pulses and electrical pulses are often required to achieve the bidirectional synaptic weight modulation.[19] In this study, the potentiation pulse is represented by a positive pulse while the depression pulse is represented by a negative pulse. Figure 2a shows that near-symmetrical potentiation and depression pulses are generated successfully under the same light intensity of visual stimuli, which will be crucial for achieving symmetrical long-term plasticity profile in synaptic devices.[20] Moreover, Figure 2a also shows that visual stimuli with greater incident light intensity result in visual V_{pre} with greater amplitude. The amplitude of visual V_{pre} is increased from 2.3 to 7.1 V when the light intensity is increased from 230 cd·m^{-2} to 672 cd·m^{-2}, suggesting a positive correlation of the input light stimuli and the generated electrical signals. This positive correlation is further quantified by plotting the visual V_{pre} amplitudes as a function of incident light intensities in Figure 2d. The data can be well fitted by a linear curve, and the detailed fitting equation can be found in Table S1. This positive and linear correlation between the incident light intensity and visual V_{pre} amplitude can be explained by the linear relationship between photocurrent and light intensity (Figure S1d).

The transduction of auditory stimuli and tactile stimuli are enabled by utilizing the same flexible polypropylene-based ferroelectret nanogenerators (FENG) but in different form

https://doi.org/10.1021/acsnano.1c04298
ACS Nano 2021, 15, 14587–14597

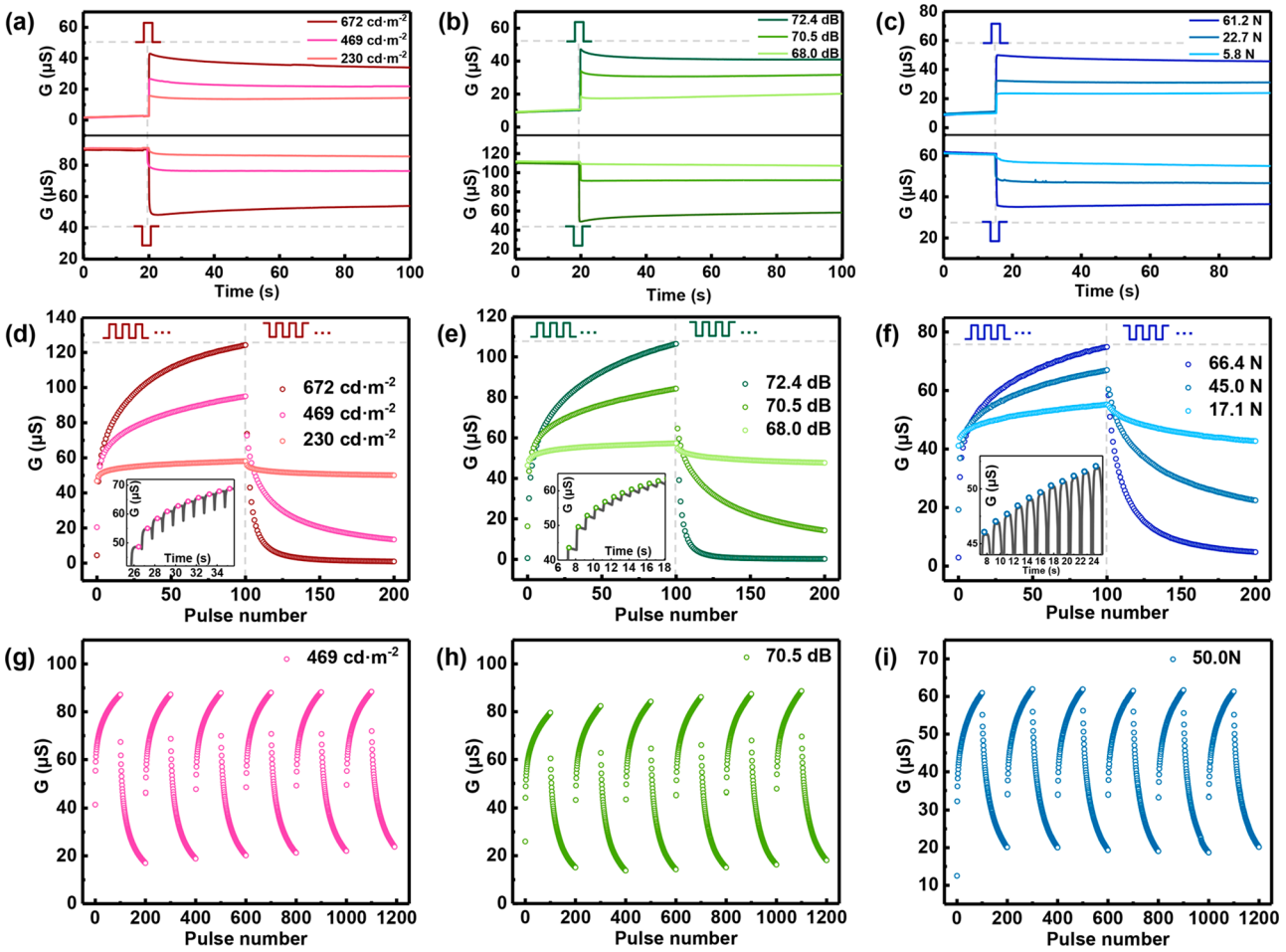

Figure 3. Single-pulse plasticity and long-term plasticity characteristics of the artificial synaptic transistor. (a–c) Single-pulse plasticity curves of synaptic transistor in response to a single potentiation or depression presynaptic pulse induced by (a) visual stimulus, (b) auditory stimulus, and (c) tactile stimulus with various stimulation intensities. (d–f) Long-term plasticity profiles of the synaptic transistor in response to a sequence of potentiation and depression presynaptic pulses (100 each for potentiation and depression) generated from (d) periodic visual stimuli with different light intensities. Inset: detailed time-domain conductance response curve (2nd to 11th pulse with a light intensity of 469 cd·m^{-2}). (e) Periodic auditory stimuli with different SPLs. Inset: detailed time-domain conductance response curve (2nd to 12th pulse with a SPL level of 70.5 dB). (f) Periodic tactile stimuli with different values of force. Inset: detailed time-domain conductance response curve (4th pulse to 14th pulse with force of 45.0 N). (g–i) Repeatability and endurance tests of synaptic transistor in response to extended period of (g) visual V_{pre}, (h) auditory V_{pre}, and (i) tactile V_{pre}.

factors and operating modes. When external mechanical perturbations are applied along the perpendicular direction to the FENG's surface, the perturbations will induce a change of internal dipole moments in the FENG, altering the electrical field distribution within the film and producing free charges at the surface electrodes, which eventually give rise to the output electrical signals. The inset of Figure 2b shows the schematic illustration of the acoustic signal transduction, where the FENG operates in a "freestanding" mode with only the four edges of the FENG fixed in a frame to allow free vibration of the film. In contrast, for transduction of tactile inputs, the FENG operates in a "blocked" mode with one side of the FENG firmly supported by a rigid substrate (inset of Figure 2c). Apart from the difference in operation modes, because the pressure induced by an acoustic signal is generally much lower compared to tactile stimulus, FENG with a larger effective area of 4 × 5 cm^2 (optical image in Figure S2b) and regulating circuit-B (circuit diagram in Figure S2a) with a much higher gain of 200 are needed to transduce and amplify the auditory stimulus. In contrast, for handling the tactile stimulus, FENG device with an effective area of 1.2 × 1.2 cm^2 (optical image in Figure S3b) and regulating circuit-C (circuit diagram in Figure S3a) with a moderate gain of 11 are used. To further demonstrate the ability of FENG to transform small auditory vibrations into noticeable electrical signals, as shown in the Figure S2d, sinusoidal sound wave with frequency of 1 kHz and sound pressure level (SPL) of 102 dB is generated by a loudspeaker and then delivered to the FENG. The pristine transduced electrical signal shows the same frequency of 1 kHz as the input sound wave and V_{pp} of near 20 mV. After amplification, the waveform retains the frequency and shows an amplified V_{pp} of near 4 V, which confirms the transduction and amplification fidelity of the acoustic FENG sensor and circuit. As illustrated in the inset of Figure 2b,c, periodical acoustic pulses with different SPLs are used as the input auditory stimuli and periodical compression with different levels of applied force are used as the input tactile stimuli, respectively. Similar to visual V_{pre} in Figure 2a, near-symmetrical potentiation and depression pulses with opposite polarities can also be generated with both auditory and tactile

https://doi.org/10.1021/acsnano.1c04298
ACS Nano 2021, 15, 14587–14597

stimuli as shown in Figure 2b,c. Figure 2b,c also shows a monotonic increase in generated electrical signals for auditory and tactile stimuli with increasing intensity. Specifically, the amplitude of generated auditory V_{pre} increases from 2.6 to 6.0 V when the SPL is increased from 68.0 to 72.4 dB and the amplitude of tactile V_{pre} increases from 3.1 to 5.4 V when the force is increased from 17.1 to 66.4 N. The amplitude of auditory V_{pre} exhibits a nonlinear relationship with SPL (Figure 2e) due to the logarithmic nature of decibel units. If the SPL is converted to the actual sound pressure using equation SPL (dB) = $20\log(P/P_0)$, where P is the sound pressure and P_0 is the reference sound pressure of 0.000 02 Pa, then the amplitude of auditory V_{pre}−P relationship can be fitted well with a linear curve (Figure S2e). The amplitudes of tactile V_{pre} as a function of the applied forces can also be fitted with a linear curve (Figure 2f). More details about the fitting equations can be found in Table S1.

As illustrated in Figure 1, after the action potentials are generated by the input sensory circuits, artificial synaptic transistors that mimick the behavior of the biological synapses are interfaced with the sensory circuits to process the action potentials. Among various neuromorphic devices, synaptic transistors based on carbon nanotube have exhibited broad conductance modulation range,[21] exceptional device scalability and uniformity,[20] outstanding flexibility,[22,23] and low energy consumption.[24−27] Due to the one-dimensional geometry and small-scale physical size of the sSWCNT, the conductance of the sSWCNT synaptic transistor is highly sensitive to charged interface trap states.[28] By controlling the charging status of the interface trap states through gate voltage pulses, the sSWCNT-based synaptic transistor can exhibit a broad conductance modulation range.[21] Also, due to the outstanding mechanical flexibility and scalability of the sSWCNT, the flexible sSWCNT synaptic transistors array with extraordinary flexibility can be fabricated on large-area, flexible substrates for potential wearable neuromorphic electronic applications.[22,23] In this research, flexible sSWCNT artificial synaptic transistors developed and reported in our previous work have been utilized.[29] Detailed synaptic characteristics of the flexible sSWCNT artificial synaptic transistor including single-pulse plasticity, spike-amplitude-dependent plasticity, spike-width-dependent plasticity, paired-pulse facilitation (PPF), and spike-time-dependent plasticity (STDP) can be found in our previous publication.[29] The optical and microscopic images of the transistor are shown in Figure S4a,b. The hysteretic transfer characteristics of the transistors that are caused by the charge trap states at the interface between the carbon nanotube and the gate oxide,[29] which lead to the synaptic behavior, are presented in Figure S4c. Key performance metrics of the synaptic transistors can be obtained and calculated from the transfer curves and the results are summarized in Table S2 of the Supporting Information. It is also worth noting that the synaptic transistor exhibits good operation stability under long-term gate biasing. 100 cycles of I_{DS}−V_{GS} curves and 100 cycles of I_{DS}−V_{DS} curves have been measured within 100 min (50 min for I_{DS}−V_{GS} and 50 min for I_{DS}−V_{DS}), and the results (Figure S5) show that both the transfer and output curves of the transistor exhibit negligible changes during the continuous, long-term reliability test.

The gate terminal of the synaptic transistor is treated as the presynaptic neuron, and the drain terminal is treated as postsynaptic neuron. With the drain-to-source voltage (V_{DS}) fixed at a constant value of −1 V, the synaptic weight of the synaptic transistor can be represented by either the drain-to-source current (I_{DS}) or the channel conductance. When a positive gate pulse is applied to the synaptic transistor, the channel conductance increases immediately and this enhancement in conductance will be maintained after the gate pulse is off. This is known as potentiation. Similarly, when a negative gate pulse is applied to the synaptic transistor, the channel conductance decreases immediately, and this degeneration will also be maintained after the gate pulse is off. This is known as depression. The changes of synaptic weight in response to different electrical pulse activations are collectively called "synaptic plasticity". Panels a, b, and c of Figure 3 show the synaptic plasticity of the sSWCNT synaptic transistor in response to a single potentiation V_{pre} and depression V_{pre} with different stimulating intensities from visual, auditory, and tactile stimuli, respectively. Before the measurements, the baselines of the channel conductance for potentiation tests are initiated to stable low conductance states ($G < 10\ \mu S$) through negative gate pulses tuning and the baselines of the channel conductance for depression tests are initiated to stable high conductance states ($G > 60\ \mu S$) through positive gate pulses tuning. After the application of single pulse, it can be seen clearly that the potentiation (positive) pulse leads to an increase in channel conductance while the depression (negative) pulse leads to a decrease in channel conductance. This phenomenon is in accordance with our previous report and confirms that positive V_{pre} will lead to potentiation while negative V_{pre} will lead to depression.[29] Furthermore, in order to study the synaptic plasticity of the synaptic transistor to the input stimulus intensity, for the same set of tests where the polarities and categories of presynaptic pulses are the same but only intensities are different, the baselines of the channel conductance are initiated at the same value before the measurements. The results in Figure 3a−c show that the physical stimulus with higher intensity can lead to greater channel conductance change and thus larger synaptic plasticity, suggesting the successful signal transmission between multimodal sensory inputs and the sSWCNT artificial synaptic transistor. In this study, the maximum conductance change in 20 s after the input pulse, noted as the ΔG_{peak}, is utilized to characterize the short-term plasticity of the synaptic transistor, whereas the average conductance change between 60 and 80 s after the input pulse, noted as ΔG_{mem}, is utilized to characterize the retention of the plasticity, which can also be seen as the "memory" of the synaptic transistor. Figure 3a shows $|\Delta G_{peak}|$ increases from 13.4 μS to 40.7 μS for potentiation and from 4.38 μS to 42.42 μS for depression when input light intensity increases from 230 cd·m^{-2} to 672 cd·m^{-2}. The corresponding $|\Delta G_{mem}|$ also increases from 12.0 μS to 32.4 μS for potentiation and from 5.27 μS to 36.4 μS for depression, which indicates a positive correlation of ΔG_{peak} and ΔG_{mem} with the incident light intensity. Similar phenomena can also be observed in Figure 3b for auditory stimulus and Figure 3c for tactile stimulus. The detailed values of ΔG_{peak} and ΔG_{mem}, as well as the retention rate, which is defined as $(\Delta G_{peak}/\Delta G_{mem}) \times 100\%$ for all three kinds of physical stimuli, are plotted in Figure S7 and summarized in Table S3. The results show that for all forms (visual, auditory, tactile) and intensities of the physical stimuli studied, over 80% for the retention rate of the single pulse plasticity can be achieved, suggesting a good synaptic-like memorization behavior of the synaptic transistor. The energy consumption for a single-pulse synaptic operation can be estimated using a simplified scheme as illustrated in

https://doi.org/10.1021/acsnano.1c04298
ACS Nano 2021, 15, 14587−14597

Figure S6a. When calculated from the single-pulse plasticity curves of single visual V_{pre} (Figure 3a), the estimated energy consumptions are in the range of tens to hundreds of nJ/per spike. However, the energy consumption of the synaptic transistor can be significantly lowered by using lower V_{DS} and by using V_{pre} with narrower pulse width (operation time). As shown in Figure S6, we have also measured the synaptic response of the transistor at V_{DS} = −5 mV with V_{pre} pulse width of 1 ms and pulse amplitude of +6 V, and such condition yields low energy consumption of several tens of fJ/per spike. More details can be found in Supporting Information ("Estimation of energy consumption in the sSWCNT artificial synaptic transistor" section), and the energy consumption values are similar to the energy consumption of actual human brain with each synaptic event consuming around 10−100 fJ.[25]

While memory can be regarded as the foundation of human intelligence, the perceptual capability of human can be further enhanced through practice or training; that is, the repetition of external stimuli in a periodic way and thus perceptual learning are enabled. In artificial sensory−memory system, such learning behavior can be preliminarily characterized by the long-term plasticity measurement, which is conducted by applying sequences of periodical potentiation and depression presynaptic pulses to the synaptic device and monitoring the modulation of channel conductance with respect to each of the input V_{pre}. Figure 3d−f shows the long-term plasticity curves of the synaptic transistor with 100 visual, auditory, and tactile potentiation and depression V_{pre}, respectively, and the insets of the Figure 3d−f show the detailed time-domain modulation curve of the synaptic transistor by visual, auditory, and tactile V_{pre}. In the measurement, the intensity of the input physical stimuli has also been varied to study the change of long-term plasticity profile under different stimulation conditions. For the tactile measurement, the force values are directly measured from the real-time readings of the commercial force sensor placed behind the FENG. During the tactile single-pulse plasticity test and long-term plasticity test, the same displacement settings of the linear motor have been used to generate similar sets of input force values. However, a slight variation may happen due to the slight movement of the scaffold or the piston, which may lead to the different force values legends in Figure 3c,f,i. In Figure 3d−f, the channel conductance starts from its minimum value (G_{min}) and then reaches the maximum value (G_{max}) after the potentiation V_{pre} sequence and gradually falls back to close to G_{min} after the depression V_{pre} sequence, suggesting a symmetrical conductance modulation profile for potentiation and depression. In Figure 3d, for input visual stimuli with light intensity of 672 cd·m^{-2}, 469 cd·m^{-2}, and 230 cd·m^{-2}, the conductance modulation range ($G_{max} - G_{min}$) is 123.2 μS, 81.6 μS, and 11.3 μS, respectively, and the on/off ratio (G_{max}/G_{min}) is 131.2, 7.07, and 1.24, respectively. For long-term plasticity measurements with auditory and tactile stimulation, the results are similar to the visual stimulation above and the detailed data for ($G_{max} - G_{min}$) and (G_{max}/G_{min}) are summarized in Table S3 in the Supporting Information. The performance of the flexible sSWCNT synaptic transistor is benchmarked with some of the previous works on synaptic transistors, and data are summarized in Table S5 in the Supporting Information. From the results above, it is clear that the V_{pre} sequences with different stimulation intensities are perceived as distinct long-term plasticity profiles by the sensory−memory system. The high-intensity long-term stimuli result in wide-range, swift tuning of the conductance with the modulation value of each step being large, whereas the low-intensity long-term stimuli show a small-range, delicate tuning profile, with the modulation value of each step being small. For potential applications in a neurorobotic system, one can utilize the change in synaptic weight (conductance or I_{DS}) of the controlling synaptic device to trigger movement of the actuator; thus different biomimetic locomotion can be enabled.[30−33] By potentially interfacing the sensory−memory system with neurorobotic actuating component, the distinct long-term plasticity profiles can be further utilized to enable different modes of actuation. As an example, according to Figure 3d, in order to achieve similar conductance tuning range from approximately 45 μS to 55 μS, one may choose to use high intensity light stimulus (672 cd·m^{-2}) to accomplish the conductance modulation from 46.53 to 55.97 μS (ΔG = 9.44 μS) with only one step (one light pulse) in the "swift mode" or to use moderate intensity light stimulus (469 cd·m^{-2}) to modulate the conductance from 46.80 μS to 56.44 μS, (ΔG = 9.81 μS) within two steps (two light pulses) in the "coarse mode". Such swift or coarse mode operation can lead to fast response and large movement of the actuator. With low intensity light stimulus (230 cd·m^{-2}), the system operates in the "fine mode" and a much more subtle adjustment of the conductance can be achieved. This allows 50 discrete conductance states or 50 steps to be established within the conductance range of 46.80−56.44 μS (ΔG = 9.64 μS), which may empower the actuator to perform slower but more intricate motion or gesture.

To further examine the electrical stability and endurance of the synaptic transistor to the V_{pre}, the long-term plasticity measurement is repeated for six cycles and the plasticity profiles of visual, auditory, and tactile stimuli are shown in panels g, h, and i of Figure 3, respectively. One thing to note is that the different initial conductance values can be attributed to the residual trapped charges from previous measurements. In the repeatability and endurance test, the initial cycle is designed to clear these trapped charges and to make the following cycles more stable. After the initial cycle, the plasticity curves are stabilized and show only slight cycle-to-cycle variations, suggesting a high modulation uniformity and operating stability of the artificial sensory−memory system. The slight increase in the maximum conductance value during the auditory repeatability and endurance test (Figure 3h) may be attributed to slight decrease of distance between the loudspeaker and FENG due to sound vibration. The sound pressure perceived by FENG will increase with decreasing distance, thus leading to the increased auditory V_{pre} and increased maximum conductance value during the test. Due to the very thin polyimide substrate (~10 μm) used and the mechanical robustness of the sSWCNT networks,[34] the long-term plasticity tests have also been successfully conducted with the synaptic transistor bent to a curvature radius of 7.5 mm. As illustrated in Figure S8a,b, the conductance modulation curves of auditory stimuli and visual stimuli exhibit only slight variations under bending state compared with relaxed state. To further demonstrate the flexibility of the transistor, the sSWCNT synaptic transistor is bent down to a very small curvature radius of 3.5 mm and the measured hysteretic transfer curves in Figure S8c show almost negligible differences. The bending test results suggest the superior mechanical flexibility of the synaptic transistor, and it may enable the potential application of the sensory−memory system in wearable electronics.

https://doi.org/10.1021/acsnano.1c04298
ACS Nano 2021, 15, 14587−14597

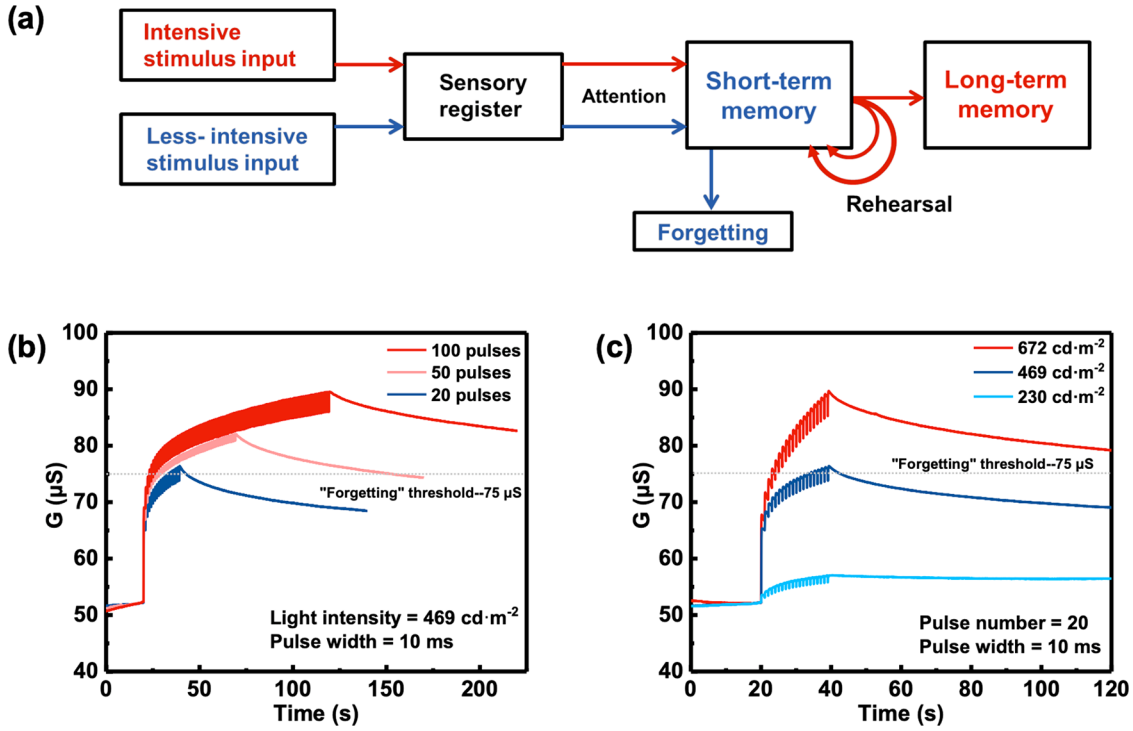

Figure 4. Electronic implementation of the multistore model, "Atkinson–Shiffrin model", of human memory by the neurological sensory–memory system. (a) Psychological model proposed by Atkinson and Shiffrin illustrating the short-term memory (STM) to long-term memory (LTM) transition in human brain. (b) Illustration of imitating STM to LTM transition through rehearsal by repeated visual stimuli. (c) Illustration of promoting STM to LTM transition through increased intensity of visual stimuli.

Beyond purely emulating the biological sensory and synaptic behaviors, the artificial neurological sensory–memory system may also be useful in implementing psychological models related to the human memory and learning process and behavior. The multistore model (Atkinson–Shiffrin model) is an explanation of human memory proposed by Atkinson and Shiffrin in 1968.[35] As shown in Figure 4a, human memory is considered to be composed of information being stored in three separate memory stages. The information detected by the sensory receptors first enters the sensory register to be stored for a very short period of time, then if attention is paid, the information in sensory register will be transferred to short-term memory (STM) for temporary memory storage, which typically has a duration of a few seconds. Through an elaborative rehearsal of the input information, the STM can be further transferred into a more long-live memory called long-term memory (LTM), and the probability of this STM–LTM conversion can be positively linked to the number of rehearsal repetitions.[36]

In the artificial neurological sensory–memory system, the loss of the memory (or the event of "forgetting") is defined as the decaying of the conductance below a certain threshold. The time span between the end of the input stimulus and the "forgetting" point is defined as the memory time (Δt_{mem}) and is going to be used to indicate the retention ability of the memory to differentiate the STM and LTM. Figure 4b illustrates the conductance change of the synaptic transistor in response to 20, 50, and 100 visual potentiation pulses, respectively, where the light intensity, pulse width, and period are set as 469 cd·m^{-2}, 10 ms, and 1 s for all three pulse sequences. A conductance of 75 μS is set as the "forgetting" threshold. For memory formed with 20 visual stimulation pulses, the conductance decays below the threshold within just a few seconds, yields a Δt_{mem} = 3.35 s, which can be classified as the STM. In contrast, for memory with 50 stimulation pulses, which corresponds to an increase in repetition of the rehearsal of the stimulus, the Δt_{mem} increases significantly to 83.4 s. For 100 pulses of stimulation, Δt_{mem} > 100 s (Δt_{mem} = 270 s, as shown in Figure S9a) is achieved, which can be regarded as LTM. Apart from the study of STM to LTM conversion through rehearsal, we also studied the effect of the stimulation intensity on this conversion. Figure 4c shows the conductance change of the synaptic transistor in response to 20 visual potentiation pulses with various light intensity of 672 cd·m^{-2}, 469 cd·m^{-2}, and 230 cd·m^{-2}, respectively. For the same conductance threshold of 75 μS, LTM with Δt_{mem} > 80 s (Δt_{mem} = 175 s, as shown in Figure S9b) is obtained with 672 cd·m^{-2} light stimuli, while STM with Δt_{mem} = 3.35 s is obtained with 469 cd·m^{-2} light stimuli. For low intensity stimulation with 230 cd·m^{-2}, the conductance fails to reach the threshold, leading to essentially Δt_{mem} = 0. In the Atkinson–Shiffrin model, information can only be transferred to the STM when sufficient attention is given to it; otherwise it is forgotten. Therefore, stimulation with greater intensity facilitates the process of sensory register to STM transition by increasing the attention level, subsequently enhancing the information retention time in short-term memory and finally resulting in the increasing of the probability of STM to LTM transformation.

The classical conditioning, represented by the experiment famously known as "Pavlov's dog experiment", is illustrated in Figure 5a. The experiment describes an associative learning process in biological brain, which occurs when a neutral/conditioned stimulus is accompanied by an unconditioned stimulus. The unconditioned stimulus to an animal is usually physiologic and innate (e.g., the appearance of the food), and it

https://doi.org/10.1021/acsnano.1c04298
ACS Nano 2021, 15, 14587–14597

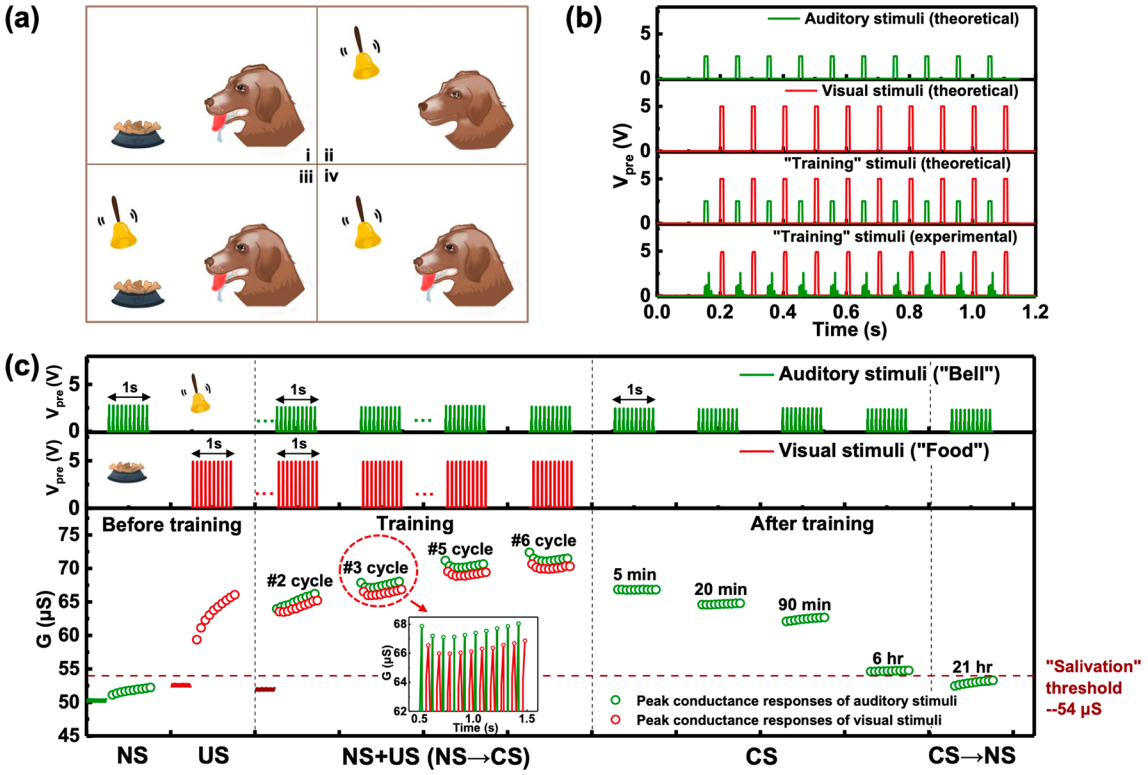

Figure 5. Electronic implementation of the classical conditioning experiment, "Pavlov's dog experiment", by the multimodal neurological sensory–memory system. (a) Schematic illustration of practical Pavlov's dog experiment. (b) Theoretical and experimental visual and auditory presynaptic pulses that are applied to the synaptic transistor to simulate the sensory responses of auditory stimuli ("bell" signals) and visual stimuli ("food" signals) in biological Pavlov's dog experiment. (c) Complete associative learning simulation with profiles of sensory responses of visual stimuli (unconditioned stimuli, US) and auditory stimuli (neutral/conditioned stimuli, NS/CS) and the corresponding synaptic transistor's channel conductance responses profile. Inset: detailed view of the channel conductance responses profile during the third training cycle.

will trigger an unconditioned response (e.g., salivation) without the necessity of learning. The conditioned stimulus, on the other hand, is a neutral stimulus (e.g., the sound of a ringing bell) in the first place. When the neutral stimulus is coupled with the unconditioned stimulus and after the neutral-unconditioned stimuli pair is repeated, the neutral stimulus alone can elicit response, which is called conditioned response, and the neutral stimulus is thus transformed into conditioned stimulus. In contrast to the rise of unconditioned response to unconditioned stimulus, the acquirement of conditioned response requires associative learning. In the Pavlov's dog experiment, the unconditioned stimulus is represented by the appearance of the food (mainly visual stimulus), which will then cause the dog to salivate even without any training. The sound from a ringing bell (mainly auditory stimulus) is initially considered as a neutral stimulus since it does not elicit salivation in the first place. During conditioning process, the food is repeatedly presented to the dog after the ringing of a bell. After the conditioning process, the sound of the bell is converted to conditioned stimulus and the dog have learned to salivate even when it only hears the sound from a bell. The successful activating of the conditioned response suggests that an association has been successfully built between the conditioned stimulus and unconditional stimulus in the animal brain by learning.

The artificial sensory–memory system provides a biomimicking approach to closely emulate the conditioning processes in Pavlov's dog's experiment. Because of the ability of the multimodal physical signal detection and processing, the visual V_{pre} can be treated as the dog's neuron-level sensory unconditioned response of the appearance of the "food", which is regarded as the unconditioned stimulus, whereas the auditory V_{pre} can be treated as neuron-level sensory conditioned response of the "ringing bell", which transits from neutral stimulus to conditioned stimulus after conditioning. The artificial synaptic transistor is considered as the synapse in the dog's brain and will convert the sensory responses to synaptic responses. As illustrated in Figure 5b, a visual V_{pre} sequence comprising 10 pulses with a pulse amplitude of 5 V, a pulse width of 10 ms, and a period of 100 ms is designed to be the sensory responses of unconditioned stimuli, while an auditory V_{pre} sequence comprising 10 pulses with a pulse amplitude of 2.5 V, a pulse width of 10 ms, and a period of 100 ms is designed to be the sensory responses of neutral/conditioned stimuli. During one training cycle, the visual V_{pre} and auditory V_{pre} in the sequence are applied alternately with an interval of 50 ms. The experimental results of the actual presynaptic pulses induced by visual and auditory stimuli are shown in the bottom panel of Figure 5b, and they exhibit close resemblance with the designed ones, indicating a successful realization of designed V_{pre} in the artificial sensory–memory system.

Figure 5c shows the comprehensive process of emulating the Pavlov's dog experiment in the artificial sensory–memory system in response to actual physical stimuli. In the experiment, the "salivation" threshold is defined as a channel

https://doi.org/10.1021/acsnano.1c04298
ACS Nano 2021, 15, 14587–14597

conductance of 54 μS. When the channel conductance reaches above this threshold, the dog is assumed to obtain the ability to salivate to the input stimuli. Before training, the neutral stimuli (auditory stimuli) result in small conductance responses that fall below the threshold, whereas the unconditioned stimuli (visual stimuli) induce significant conductance responses that exceed the salivation threshold ("before training" phase in Figure 5c). During the training process, a total of six cycles of training sequences are applied, and the conductance responses profile suggests that an association of the neutral stimuli and unconditioned stimuli is being established. A detailed view of the conductance responses profile during the third training cycle is shown in the inset of the "training" phase plot. After training is completed, due to the synaptic memory that the transistor acquired during the training process, the synaptic transistor can reach above the "salivation" threshold when the auditory stimuli are given alone without the existence of visual stimuli. This phenomenon suggests that correlation of the neutral stimuli and unconditioned stimuli has been built which leads to the transition of the neutral stimuli to the conditioned stimuli by successfully triggering the conditioned responses. It is also worth noting that the conditioned responses are less permanent than unconditioned responses. In the "after training" phase, the conditioned conductance responses induced by conditioned (auditory) stimuli gradually decay over an extended period of time and eventually drop below the "salivation" threshold after 21 h, which indicates that the conditioned stimuli have transited back to neutral stimuli. This can be understood as the conditioned response, and the neutral stimulus-conditioned stimulus conversion and association are obtained by learning and memory, and the memory can fade over time if it is not rehearsed according to the Atkinson–Shiffrin model. However, the neutral stimulus-conditioned stimulus association can always be rebuilt, or even strengthened, by additional retraining.

CONCLUSION

We have presented a multimodal artificial sensory–memory system that possesses the biomimicking sensory transduction and neurological, synapse-like information processing and memorizing capabilities. Successful transduction of visual, auditory, and tactile stimuli into pulsed, information-containing electrical presynaptic pulses has been achieved through sensors such as phototransistor and FENG in acoustic sensor mode and force sensor mode. The synaptic plasticity of the flexible sSWCNT artificial synaptic transistor has been studied by inducing single-pulse plasticity and long-term plasticity with single pulse and sequence of presynaptic pulses including by actual physical stimuli. The synapse-like processing and memory behavior, tunable long-term synaptic plasticity profile, and cycle-to-cycle modulation stability have all been demonstrated. Empowered by this artificial sensory–memory system, electronic analogues of two famous psychological models and experiments of brain memory and learning are implemented. The "multistore model" shows the STM to LTM transition with increased light-stimuli rehearsal and intensity. A bioplausible classical conditioning experiment ("Pavlov's dog experiment") is also successfully implemented by integrating actual visual stimuli (physical representation of the image of "food") and actual auditory stimuli (physical representation of the sound of "bell") in the synaptic transistor to enable the imitation of associative learning behavior. The multimodal artificial sensory–memory system demonstrated in this study can potentially widen the application scenario of the artificial intelligence by introducing environment-interactive functions and may also find applications in fields such as cyborg systems and neuroprosthetics.

METHODS

Fabrication Process of Flexible Carbon Nanotube Synaptic Transistor. Polyimide (HD Microsystems) thin film is spin-coated (step 1, 1000 rpm, 30 s; step 2, 2000 rpm, 1 min) on Si wafer and heated by a hot plate (300 °C, 10 min). Bottom-gate electrodes (Ti/Au, 5/30 nm) are first fabricated by photolithography and lift-off, then the dielectric layers (Al_2O_3/SiO_x, 20/15 nm) are deposited by atomic layer deposition (ALD) and e-beam evaporation. The functionalized (poly-L-lysine, 0.1% w/v, Sigma-Aldrich) and rinsed sample is subsequently immersed into sSWCNT solution (0.01 mg/mL, NanoIntegris Inc., 15 min) for active channel material deposition. After cleaning by DI water and isopropyl alcohol (IPA), the sample is blow-dried and annealed in vacuum oven (200 °C, 10 min) to remove surfactant residues. After that, the drain and source electrodes (Ti/Pd, 0.5/35 nm) are formed by photolithography and e-beam evaporation and the fabrication of the transistors is finalized by last step of photolithography and oxygen plasma to remove sSWCNT networks outside the drain-source-defined channel region. After the fabrication process is completed, the four edges of the polyimide substrate are cut by a razor blade and the synaptic transistors array on the polyimide substrate is carefully delaminated from the handling silicon wafer by tweezers.

Fabrication of Flexible Ferroelectret Nanogenerator. The PPFE film (80 μm in thickness, Emfit Corporation) is sputter-coated with Ag film (500 nm, Hummer X, Anatech Inc.) on each side. After the deposition of the two Ag electrodes, they are wired out through copper wires and tapes. For the acoustic sensor application, only the Ag electrode–copper wire connection area is covered with polyimide film (20 μm, Kapton) as protection layer. For the force sensor application, the whole FENG device is encapsulated by the polyimide film as protection layer.

Visual Stimulus Generation and Detection. The pulsed signals are generated by Keysight 33510B waveform generator and sent to a white light LED (⌀ = 5 mm, US-EL-CP-010, ELEGOO) to generate pulsed visual stimuli. The ambient light phototransistor (⌀ = 5 mm, ALS-PT243-3C/L177, EVERLIGHT) is placed 43 mm away from the LED to transduce the visual stimuli, and a photometer (1330B-V digital light meter, DR. METER) is placed at the same position as the phototransistor to monitor the input light intensities of the visual stimuli. The visual presynaptic pulses are measured and recorded by an oscilloscope (Analog Discovery 2, DIGILENT) at a sample rate of 400 Hz.

Auditory Stimulus Generation and Detection. The pulsed signals are generated by Keysight 33510B waveform generator and sent to a loudspeaker (⌀ = 3 in., HiFi full-range, DROK) to generate pulsed auditory stimuli. The FENG film (4 × 5 cm^2 effective area) is attached to a scaffold (as shown in Figure S2c) with an open window (4 × 5 cm^2) and aligned with the center of the loudspeaker and is placed 2 cm away from the loudspeaker. A decibel meter (HT-80A decibel meter, RISEPRO) is placed at the same position as the FENG to monitor the input SPLs of the auditory stimuli. The auditory presynaptic pulses are measured and recorded by an oscilloscope (Analog Discovery 2, DIGILENT) at a sample rate of 800 Hz.

Tactile Stimulus Generation and Detection. The PI-encapsulated FENG (1.2 × 1.2 cm^2 effective area) is mounted on a fixed scaffold and is aligned with a rubber piston (1.2 × 1.2 cm^2 front area) mounted on a linear motor (Legato 110 syringe pump, kd Scientific). The loading test setup is shown in Figure S3c. During the experiment, the rubber piston will be brought in contact with the FENG periodically with preset frequency and moving distance, generating pulsed compressive tactile stimuli. A commercial force sensor (⌀ = 0.5 in., force sensing resistor, POLOLU, shown in Figure S3d) is placed in tandem with the FENG to measure the magnitude of the applied force. The tactile presynaptic pulses are measured and

https://doi.org/10.1021/acsnano.1c04298
ACS Nano 2021, 15, 14587–14597

recorded by an oscilloscope (Analog Discovery 2, DIGILENT) at sample rate of 400 Hz.

Synaptic Response Measurement and Sensory−Memory System Characterization. After the visual, auditory, or tactile presynaptic pulses are sent to the artificial synaptic transistor for processing, the changes of the synaptic weight of the synaptic transistor are measured by a semiconductor device analyzer (Keysight B1500A) in the form of I_{DS} or channel conductance at fixed V_{DS} of −1 V. All synaptic measurements except the long-term plasticity tests at bending radius of 7.5 mm are conducted on synaptic transistor with L = 10 μm, W = 200 μm. The long-term plasticity tests at bending radius of 7.5 mm are conducted on synaptic transistor with L = 10 μm, W = 100 μm.

ASSOCIATED CONTENT

Supporting Information

The Supporting Information is available free of charge at https://pubs.acs.org/doi/10.1021/acsnano.1c04298.

Multimodal sensory system circuit and device diagrams; characterization of presynaptic action potentials; characteristics of the sSWCNT artificial synaptic transistor; stability and reliability test of the sSWCNT artificial synaptic transistor; estimation of energy consumption in the sSWCNT artificial synaptic transistor; single-pulse plasticity and long-term plasticity characterizations; mechanical flexibility test of the sSWCNT artificial synaptic transistor; retention time measurement of the LTM in multistore model; comparison of flexible sSWCNT synaptic transistor and other synaptic devices (PDF)

AUTHOR INFORMATION

Corresponding Author

Chuan Wang − *Electrical and Systems Engineering and Institute of Materials Science and Engineering, Washington University in St. Louis, St. Louis, Missouri 63130, United States;* orcid.org/0000-0002-5296-0631; Email: chuanwang@wustl.edu

Authors

Haochuan Wan − *Electrical and Systems Engineering, Washington University in St. Louis, St. Louis, Missouri 63130, United States*

Junyi Zhao − *Electrical and Systems Engineering, Washington University in St. Louis, St. Louis, Missouri 63130, United States*

Li-Wei Lo − *Electrical and Systems Engineering and Institute of Materials Science and Engineering, Washington University in St. Louis, St. Louis, Missouri 63130, United States*

Yunqi Cao − *State Key Laboratory of Industrial Control Technology, College of Control Science and Engineering, Zhejiang University, Hangzhou, Zhejiang 310027, China*

Nelson Sepúlveda − *Electrical and Computer Engineering, Michigan State University, East Lansing, Michigan 48824, United States;* orcid.org/0000-0002-9676-8529

Complete contact information is available at: https://pubs.acs.org/10.1021/acsnano.1c04298

Notes

The authors declare no competing financial interest.

ACKNOWLEDGMENTS

This work was partially funded by Washington University and a Michigan State University Foundation Strategic Partnership Grant (No. 16-SPG-Full-3236). The authors acknowledge the Washington University Institute of Materials Science and Engineering for the use of instruments and staff assistance.

REFERENCES

(1) Wan, C.; Cai, P.; Wang, M.; Qian, Y.; Huang, W.; Chen, X. Artificial Sensory Memory. *Adv. Mater.* **2020**, *32*, 1902434.

(2) Kim, Y.; Chortos, A.; Xu, W.; Liu, Y.; Oh, J. Y.; Son, D.; Kang, J.; Foudeh, A. M.; Zhu, C.; Lee, Y.; et al. A Bioinspired Flexible Organic Artificial Afferent Nerve. *Science* **2018**, *360*, 998−1003.

(3) Sun, F.; Lu, Q.; Feng, S.; Zhang, T. Flexible Artificial Sensory Systems Based on Neuromorphic Devices. *ACS Nano* **2021**, *15*, 3875−3899.

(4) Jung, Y. H.; Park, B.; Kim, J. U.; Kim, T. i. Bioinspired Electronics for Artificial Sensory Systems. *Adv. Mater.* **2019**, *31*, 1803637.

(5) Gu, L.; Poddar, S.; Lin, Y.; Long, Z.; Zhang, D.; Zhang, Q.; Shu, L.; Qiu, X.; Kam, M.; Javey, A.; Fan, Z. A Biomimetic Eye with a Hemispherical Perovskite Nanowire Array Retina. *Nature* **2020**, *581*, 278−282.

(6) Mennel, L.; Symonowicz, J.; Wachter, S.; Polyushkin, D. K.; Molina-Mendoza, A. J.; Mueller, T. Ultrafast Machine Vision with 2D Material Neural Network Image Sensors. *Nature* **2020**, *579*, 62−66.

(7) Seo, S.; Jo, S.-H.; Kim, S.; Shim, J.; Oh, S.; Kim, J.-H.; Heo, K.; Choi, J.-W.; Choi, C.; Oh, S.; et al. Artificial Optic-Neural Synapse for Colored and Color-Mixed Pattern Recognition. *Nat. Commun.* **2018**, *9*, 5106.

(8) Sun, J.; Oh, S.; Choi, Y.; Seo, S.; Oh, M. J.; Lee, M.; Lee, W. B.; Yoo, P. J.; Cho, J. H.; Park, J. H. Optoelectronic Synapse Based on Igzo-Alkylated Graphene Oxide Hybrid Structure. *Adv. Funct. Mater.* **2018**, *28*, 1804397.

(9) Wang, C.; Hwang, D.; Yu, Z.; Takei, K.; Park, J.; Chen, T.; Ma, B.; Javey, A. User-Interactive Electronic Skin for Instantaneous Pressure Visualization. *Nat. Mater.* **2013**, *12*, 899−904.

(10) Shi, H.; Al-Rubaiai, M.; Holbrook, C. M.; Miao, J.; Pinto, T.; Wang, C.; Tan, X. Screen-Printed Soft Capacitive Sensors for Spatial Mapping of Both Positive and Negative Pressures. *Adv. Funct. Mater.* **2019**, *29*, 1809116.

(11) Fan, F. R.; Tang, W.; Wang, Z. L. Flexible Nanogenerators for Energy Harvesting and Self-Powered Electronics. *Adv. Mater.* **2016**, *28*, 4283−4305.

(12) Fan, F.-R.; Tian, Z.-Q.; Wang, Z. L. Flexible Triboelectric Generator. *Nano Energy* **2012**, *1*, 328−334.

(13) Li, W.; Torres, D.; Wang, T.; Wang, C.; Sepúlveda, N. Flexible and Biocompatible Polypropylene Ferroelectret Nanogenerator (Feng): On the Path toward Wearable Devices Powered by Human Motion. *Nano Energy* **2016**, *30*, 649−657.

(14) Luo, Z.; Zhu, D.; Shi, J.; Beeby, S.; Zhang, C.; Proynov, P.; Stark, B. Energy Harvesting Study on Single and Multilayer Ferroelectret Foams under Compressive Force. *IEEE Trans. Dielectr. Electr. Insul.* **2015**, *22*, 1360−1368.

(15) Cao, Y.; Figueroa, J.; Pastrana, J. J.; Li, W.; Chen, Z.; Wang, Z. L.; Sepúlveda, N. Flexible Ferroelectret Polymer for Self-Powering Devices and Energy Storage Systems. *ACS Appl. Mater. Interfaces* **2019**, *11*, 17400−17409.

(16) Cao, Y.; Figueroa, J.; Li, W.; Chen, Z.; Wang, Z. L.; Sepúlveda, N. Understanding the Dynamic Response in Ferroelectret Nanogenerators to Enable Self-Powered Tactile Systems and Human-Controlled Micro-Robots. *Nano Energy* **2019**, *63*, 103852.

(17) Li, W.; Torres, D.; Díaz, R.; Wang, Z.; Wu, C.; Wang, C.; Wang, Z. L.; Sepúlveda, N. Nanogenerator-Based Dual-Functional and Self-Powered Thin Patch Loudspeaker or Microphone for Flexible Electronics. *Nat. Commun.* **2017**, *8*, 15310.

(18) Bi, G.-q.; Poo, M.-m. Distributed Synaptic Modification in Neural Networks Induced by Patterned Stimulation. *Nature* **1999**, *401*, 792−796.
(19) Subramanian Periyal, S.; Jagadeeswararao, M.; Ng, S. E.; John, R. A.; Mathews, N. Halide Perovskite Quantum Dots Photosensitized-Amorphous Oxide Transistors for Multimodal Synapses. *Adv. Mater. Technol.* **2020**, *5*, 2000514.
(20) Sanchez Esqueda, I.; Yan, X.; Rutherglen, C.; Kane, A.; Cain, T.; Marsh, P.; Liu, Q.; Galatsis, K.; Wang, H.; Zhou, C. Aligned Carbon Nanotube Synaptic Transistors for Large-Scale Neuromorphic Computing. *ACS Nano* **2018**, *12*, 7352−7361.
(21) Kim, S.; Yoon, J.; Kim, H.-D.; Choi, S.-J. Carbon Nanotube Synaptic Transistor Network for Pattern Recognition. *ACS Appl. Mater. Interfaces* **2015**, *7*, 25479−25486.
(22) Kim, S.; Choi, B.; Lim, M.; Yoon, J.; Lee, J.; Kim, H.-D.; Choi, S.-J. Pattern Recognition Using Carbon Nanotube Synaptic Transistors with an Adjustable Weight Update Protocol. *ACS Nano* **2017**, *11*, 2814−2822.
(23) Yang, K.; Yuan, S.; Huan, Y.; Wang, J.; Tu, L.; Xu, J.; Zou, Z.; Zhan, Y.; Zheng, L.; Seoane, F. Tunable Flexible Artificial Synapses: A New Path toward a Wearable Electronic System. *npj Flexible Electron.* **2018**, *2*, 20.
(24) Kim, K.; Chen, C. L.; Truong, Q.; Shen, A. M.; Chen, Y. A Carbon Nanotube Synapse with Dynamic Logic and Learning. *Adv. Mater.* **2013**, *25*, 1693−1698.
(25) Feng, P.; Xu, W.; Yang, Y.; Wan, X.; Shi, Y.; Wan, Q.; Zhao, J.; Cui, Z. Printed Neuromorphic Devices Based on Printed Carbon Nanotube Thin-Film Transistors. *Adv. Funct. Mater.* **2017**, *27*, 1604447.
(26) Wang, Y.; Huang, W.; Zhang, Z.; Fan, L.; Huang, Q.; Wang, J.; Zhang, Y.; Zhang, M. Ultralow-Power Flexible Transparent Carbon Nanotube Synaptic Transistors for Emotional Memory. *Nanoscale* **2021**, *13*, 11360−11369.
(27) Zhao, J.; Liu, F.; Huang, Q.; Lu, T.; Xi, M.; Peng, L.; Liang, X. Charge Trap-Based Carbon Nanotube Transistor for Synaptic Function Mimicking. *Nano Res.* **2021**, 1−6.
(28) Bushmaker, A. W.; Oklejas, V.; Walker, D.; Hopkins, A. R.; Chen, J.; Cronin, S. B. Single-Ion Adsorption and Switching in Carbon Nanotubes. *Nat. Commun.* **2016**, *7*, 10475.
(29) Wan, H.; Cao, Y.; Lo, L.-W.; Zhao, J.; Sepulveda, N.; Wang, C. Flexible Carbon Nanotube Synaptic Transistor for Neurological Electronic Skin Applications. *ACS Nano* **2020**, *14*, 10402−10412.
(30) Lee, Y.; Oh, J. Y.; Xu, W.; Kim, O.; Kim, T. R.; Kang, J.; Kim, Y.; Son, D.; Tok, J. B.-H.; Park, M. J.; Bao, Z.; Lee, T.-W. Stretchable Organic Optoelectronic Sensorimotor Synapse. *Sci. Adv.* **2018**, *4*, eaat7387.
(31) Akbari, M. K.; Zhuiykov, S. A Bioinspired Optoelectronically Engineered Artificial Neurorobotics Device with Sensorimotor Functionalities. *Nat. Commun.* **2020**, *10*, 1−10.
(32) He, K.; Liu, Y.; Wang, M.; Chen, G.; Jiang, Y.; Yu, J.; Wan, C.; Qi, D.; Xiao, M.; Leow, W. R.; et al. An Artificial Somatic Reflex Arc. *Adv. Mater.* **2020**, *32*, 1905399.
(33) Shim, H.; Sim, K.; Ershad, F.; Yang, P.; Thukral, A.; Rao, Z.; Kim, H.-J.; Liu, Y.; Wang, X.; Gu, G.; et al. Stretchable Elastic Synaptic Transistors for Neurologically Integrated Soft Engineering Systems. *Sci. Adv.* **2019**, *5*, eaax4961.
(34) Wang, C.; Chien, J.-C.; Takei, K.; Takahashi, T.; Nah, J.; Niknejad, A. M.; Javey, A. Extremely Bendable, High-Performance Integrated Circuits Using Semiconducting Carbon Nanotube Networks for Digital, Analog, and Radio-Frequency Applications. *Nano Lett.* **2012**, *12*, 1527−1533.
(35) Atkinson, R. C.; Shiffrin, R. M. Human Memory: A Proposed System and Its Control Processes. In *Psychology of Learning and Motivation*; Elsevier, 1968; Vol. *2*, pp 89−195.
(36) Ohno, T.; Hasegawa, T.; Tsuruoka, T.; Terabe, K.; Gimzewski, J. K.; Aono, M. Short-Term Plasticity and Long-Term Potentiation Mimicked in Single Inorganic Synapses. *Nat. Mater.* **2011**, *10*, 591−595.

https://doi.org/10.1021/acsnano.1c04298
ACS Nano 2021, 15, 14587−14597